ATMOSPHERIC ENVIRONMENT: X 21 (2024) 100245

Contents lists available at ScienceDirect

Atmospheric Environment: X

journal homepage: www.journals.elsevier.com/atmospheric-environment-x

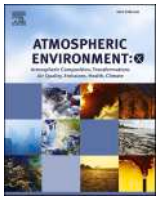

3D numerical simulation of airflow structure and dust emissions from an open storage pile behind a dynamic solid fence-deflector

Ouiza Bouarour [a,*], Aonghus McNabola [b], Battista Grosso [a], Brian Considine [b], Alessio Lai [a], Francesco Pinna [a], Valentina Dentoni [a]

[a] Department of Civil and Environmental Engineering and Architecture, University of Cagliari, Via Marengo, 2, 09123, Cagliari, Italy
[b] Department of Civil, Structural & Environmental Engineering, Trinity College Dublin, Dublin, D02 PN40, Ireland

ARTICLE INFO

Keywords:
Open storage yards
Dust emission
Solid fence
Dynamic deflector
Numerical simulation

ABSTRACT

Open storage yards at industrial sites represent a significant fugitive dust emission source. Granular material subjected to wind erosion may emit significant dust into the atmosphere. Several windbreaks and fences with different shapes have been proposed to control and reduce those emissions. Solid fences are commonly erected around the open yard (i.e., open bays) to prevent and reduce those emissions, even though they have some limitations. The present study aims to enhance the effectiveness of solid fences by coupling them with dynamic wind deflectors. Computational fluid dynamics was employed to simulate the flow and shear stresses on storage pile surfaces using the numerical Reynolds-averaged Navier–Stokes equations and the *k-ω SST* turbulence model. At the same time, dust emission was estimated using an Environmental Protection Agency (EPA) method, which estimates the emission potential of a material based on the wind friction velocity and the material's threshold friction velocity. The numerical model was validated against experimental data from an EPA study. In addition, this study investigated the efficiency of various dynamic wind deflectors with different heights and inclination angles. The results showed that most of the investigated dynamic fence-deflector models reduced the velocity magnitude, vortices, and turbulence intensity, lessening the impact of shear stresses compared to single solid fences and consequently reducing the emission of dust from the exposed surfaces (i.e., a primary measure of impact reduction). More specifically, the deflector of width (Y_{def}) 2 m with an inclination of ($\varnothing_{def}$) 65° was the most effective, where the shear stress on the pile surface and the emission factor were reduced by 29.16% and 21.79%, respectively, compared to the single fence of the same height. Finally, adding dynamic wind deflectors enhances the performance of solid fences, and it is a more effective and less expensive solution than replacing single fences with other windbreak models.

1. Introduction

Dust emissions result from wind action on exposed erodible materials (wind erosion) and represent an essential and significant part of the overall emission from industrial sites. A typical example of industrial wind erosion sources is the open storage piles of granular materials (raw materials, semi, and final products), usually left uncovered due to the frequent transfer of material from/to stockyards. Those emissions cause environmental problems (e.g., degradation of air quality), risks to human health, and material losses for industries. Dust emissions from stockpiles of granular materials depend mainly on the physical and chemical characteristics of the materials and those of the incident wind (Dentoni et al., 2022). The Environmental Protection Agency (EPA) suggested a method which estimates the emission potential of a material based on the threshold shear velocity (the velocity at which the emission starts) of the specific granular material and on the wind friction velocity (U.S. EPA, 2006). In order to apply the EPA procedure, the wind field around the stockpile needs to be derived. Several authors have used Computational Fluid Dynamics (CFD) simulations to obtain wind field information for use in the EPA procedure. Diverse simulations encompassed the prediction of wind flow patterns over isolated piles with varying geometries, including semi-circular (Diego et al., 2009; Torano et al., 2007), oblong with flat (Turpin and Harion, 2010) or sharp crests (Badr and Harion, 2007; M. Ferreira et al., 2020; Furieri et al., 2012), and rectangular/square piles (Badas et al., 2022). Additionally, researchers have delved into the numerical prediction of dust emissions

* Corresponding author. Department of Civil and Environmental Engineering and Architecture, University of Cagliari, Via Marengo, 2, 09123, Cagliari, Italy.
E-mail address: o.bouarour@studenti.unica.it (O. Bouarour).

https://doi.org/10.1016/j.aeaoa.2024.100245
Received 3 November 2023; Received in revised form 6 February 2024; Accepted 19 February 2024
Available online 21 February 2024
2590-1621/© 2024 The Authors. Published by Elsevier Ltd. This is an open access article under the CC BY-NC-ND license (http://creativecommons.org/licenses/by-nc-nd/4.0/).

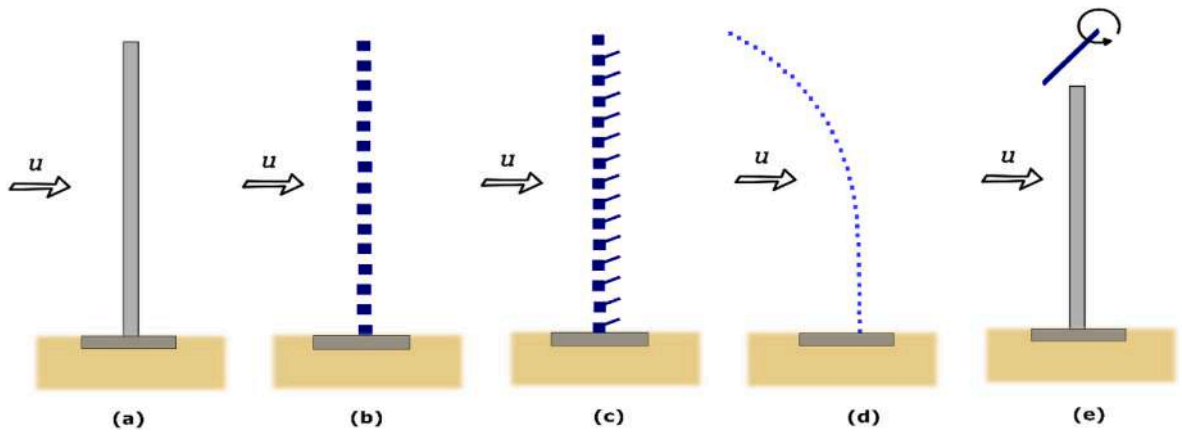

Fig. 1. Profiles of the existing wind fences (a) solid fence, b) porous fence, c) deflector-porous fence (Chen et al., 2012), d) porous fences with curved deflectors (Qiu et al., 2022) and (e) the new dynamic fence-deflector.

from successive parallel stockpiles (Diego et al., 2009; Furieri et al., 2012; Ferreira et al., 2020) or from open yards with complex geometry, emphasising factors such as surrounding buildings (Turpin and Harion, 2010) and stockpile layout configurations (Cong et al., 2012; Novak et al., 2015).

Several technical strategies and management measures have been used to reduce fugitive dust emissions and particulate matter (PM) dispersion into the atmosphere, including applying water or chemical suppressants (Yen et al., 2021) covering the material with tarps, or storing the material in enclosures (Hassan et al., 2017; Yonkofski et al., 2019). Storing the material in enclosures and erecting wind barriers (e.g., erecting a 3-sided enclosure around storage piles) is widely used as a control measure to reduce windblown fugitive dust from uncovered material stockpiles (WRAP, 2006). Those wind barriers rapidly and significantly impact the shelter effect (LV et al., 2013). The barriers reduce wind speed and momentum by blocking the wind path, reducing wind erosion and dust emission (Torshizi et al., 2020).

Researchers have conducted numerous experimental field tests and wind tunnel experiments to investigate the performance and efficiency of wind fences on open storage piles (Lee and Lim, 2001; Ning et al., 2011). Other authors have used CFD modeling to obtain similar results. Lee and Lim (2001) conducted a numerical analysis to examine the shelter effect of the porous wind fence on wind flow around a triangular prism model, considering the porosity, height, and location of the wind fence as variables. Regarding the results, the wind fence with a 30–50% porosity was the most effective in reducing the mean pressures acting on the stockpile surface and turbulent kinetic energy in the fence wake. Chen et al. (2012) performed a 3D numerical study to simulate the flow field around a triangular-shaped prism model behind the newly introduced deflector-porous fence. This new type of porous fence has been designed to weaken the effect of the bleed flow on the windward side of the stockpiles. The study results show that the deflector-porous fence, with a porosity of 30% and a height and location of 150 mm, is the most efficient fence to control dust emissions. A numerical study conducted by Song et al. (2014) gives more detailed information on the airflow fields behind porous fences by studying the internal relations between the sheltering effect and the shear stress distribution on each surface of the storage pile. This study indicated that a fence with a porosity between 20 % and 30 % is optimal. To summarize, all three studies aimed to reduce the impact of wind around stockpiles (triangular models by Lee and Lim (2001), Chen et al. (2012), and the flat-top prismatic model by Song et al. (2014)). They utilize porous wind fences with different porosities, heights, and locations. Despite their diverse designs and specific focuses, these studies agree on the significance of porosity in achieving optimal performance for wind fences in controlling airflow around stockpiles.

The investigation extends to alternative open bay geometries, such as isolated stockpiles stacked against three walls (Badas et al., 2022).To explore the influence of wind-porous fences on open storage piles, various studies focus on the shelter effect of porous wind fences, considering variables like porosity, height, and location (Chen et al., 2012; A. D. Ferreira and Lambert, 2011; San et al., 2019; Song et al., 2014). While recent innovations, such as curved deflectors Qiu et al. (2021, 2022), aim to enhance the effectiveness of these protective structures. Through these multifaceted simulations, researchers aim to contribute valuable insights into the dynamics of wind flow and fugitive dust, which is crucial for addressing environmental concerns in diverse industrial settings.

Despite the diverse studies attesting to the high performance of porous fences in reducing dust emission compared to solid ones, solid fences are still widely used in industrial areas and ports as enclosures or windbreaks for open storage piles. Furthermore, solid fences are commonly used in arid regions to prevent sand deposition and drift (Alghamdi and Al-Kahtani, 2005). Moreover, solid fences are more effective than porous fences in reducing wind speed. However, the rapid decrease in the sheltered area behind the fence (Dong et al., 2007) and the sand accumulation and sedimentation at the windward side of the solid fences (Bruno et al., 2018; Dong et al., 2006) can be considered as problematic for solid fences.

To our knowledge, solid fences are scarcely investigated in the literature compared with the numerous studies about porous fences. Besides, the previous works have not considered the economic aspect in investigating management methods to improve the efficiency of solid fences in preventing open storage dust emissions (e.g. the economic impact of replacing the solid fences already implemented with other windbreak structures).

Considering the need to enhance the zero porosity fences' efficiency, the present study aims to investigate the design and performance of dynamic wind deflectors to be coupled with solid fences to control and reduce dust emissions.

The dynamic deflector was designed as an attachment to solid fences which can move its angle according to the pile height, wind speed, or direction changes to ensure optimal protection for the pile and effective reduction of dust emission. As such, a new design termed a dynamic fence-deflector is proposed in this study.

2. Materials and methods

2.1. Numerical case description

For the current work, three-dimensional (3D) simulations have been conducted using the commercial CFD software ANSYS FLUENT to assess

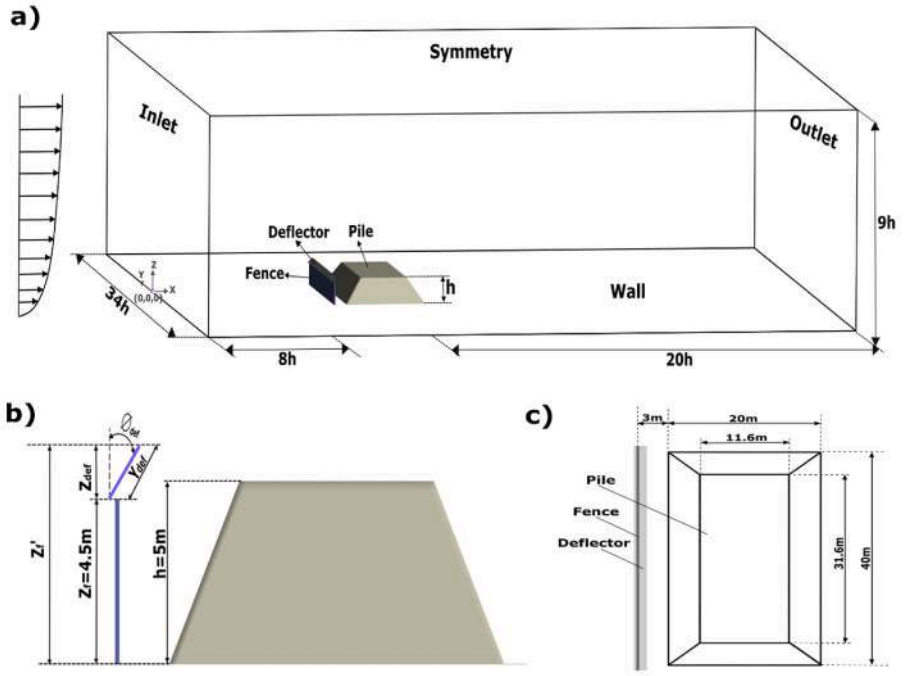

Fig. 2. Description of a) the computational flow domain sizes and boundary conditions, b) lateral view of the modelled pile and solid fence-deflector, and c) top view of the pile dimension.

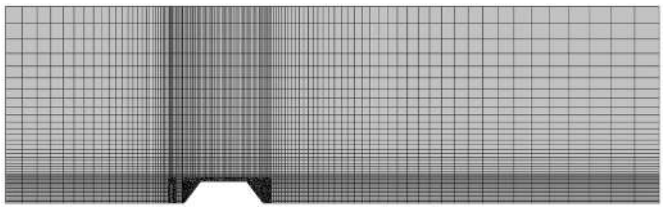

Fig. 3. Grid system used in this study.

the effectiveness of implementing wind deflectors on the top of solid fences installed behind an open storage pile to reduce dust emissions. It should be noted that this study focuses on the flow field properties without considering the solid particles effect on turbulence. In addition, all simulations in the study were also performed under the same wind profile with a reference value of 5 m/s.

Fig. 1 shows the existing fences used to reduce dust emissions from open storage. Profile (e) in Fig. 1 represents the proposed dynamic fence-deflector profile.

The deflector is installed on the top of a solid fence of a height Z_f = 4.5 m, as shown in Figs. 1(e) and Fig. 2(b). The deflector was designed to move its angle in response to changes in pile height, wind speed or direction. This concept of a dynamic deflector was considered by simulating three inclination angles ($\varnothing_{def} = 35°$, 50° and 65°). For each angle, five deflector heights (Y_{def}) were tested (0.5, 0.8, 1, 1.5 and 2 m) as shown in Fig. 2(b). Additionally, the dust control efficiency of five wind deflectors (chosen randomly from the 15 simulated cases) were compared to five additional single solid fences having the same height (Z_f') as the fence-deflector. This assessed whether the proposed dynamic fence-deflector performs better than a single solid fence.

2.2. Mathematical model description

This research evaluated the dynamic fence-deflector efficiency by assessing the shear stress distribution over the pile surfaces and then estimating the emission factor (EF) using the USEPA model.

Section 13.2.5 of the AP-42 Compilation of Air Pollutant Emission Factors published by the United States Environmental Protection Agency (U.S. EPA, 2006) recommends using the following emission factor to estimate wind erosion emissions from a stockpile:

$$EF = m \sum_{i=1}^{N} \sum_{j=1}^{M} P_{ij} \cdot S_{ij} \quad (1)$$

where m is a particle size multiplier (equal to 0.5 for PM_{10} (U.S. EPA, 2006), N is the total number of disturbances per year, M is the number of the sub-areas having a constant value of u_s/u_r, P_{ij} is the erosion potential (g/m^2), and S_{ij} (m^2) is the fraction of the subarea corresponding to a constant value of u_s/u_r.

The erosion potential is defined as:

$$P = 58\left(u^* - u_t^*\right)^2 + 25\left(u^* - u_t^*\right), for\ u^* \geq u_t^* \quad (2)$$

P = 0, for $u^* \leq u_t^*$ where u_t^* is the threshold velocity and u^* is given by the following equation,

$$u^* = 0.1\, u_{10}^+ \cdot (u_s\ /\ u_r) \quad (3)$$

where u_{10}^+ is the fastest mile of wind speed measured at 10 m height, u_s is the average wind speed at 25 cm from the pile surface and u_r is the average wind speed (reference value) at 10 m above terrain.

For this work, it was assumed that there was only one disturbance per year ($N = 1$), and the simulation adopted a reference value of $u_t^* = 0$ m/s for the most conservative estimation. These assumptions were in line with previous studies of this nature (Yeh et al., 2010). Therefore, Equations (1) and (2) become as follows,

$$EF_0 = 0.5 \sum_{j=1}^{M} P_{0j} \bullet S_j \quad (4)$$

$$P_0 = 58\, u^{*2} + 25\, u^* \quad (5)$$

Then, according to Equation (4), the whole pile surface was divided into different sub-areas of constant u_s/u_r. Each sub-area was considered a single source, where u_s/u_r ratios were obtained by CFD calculation and

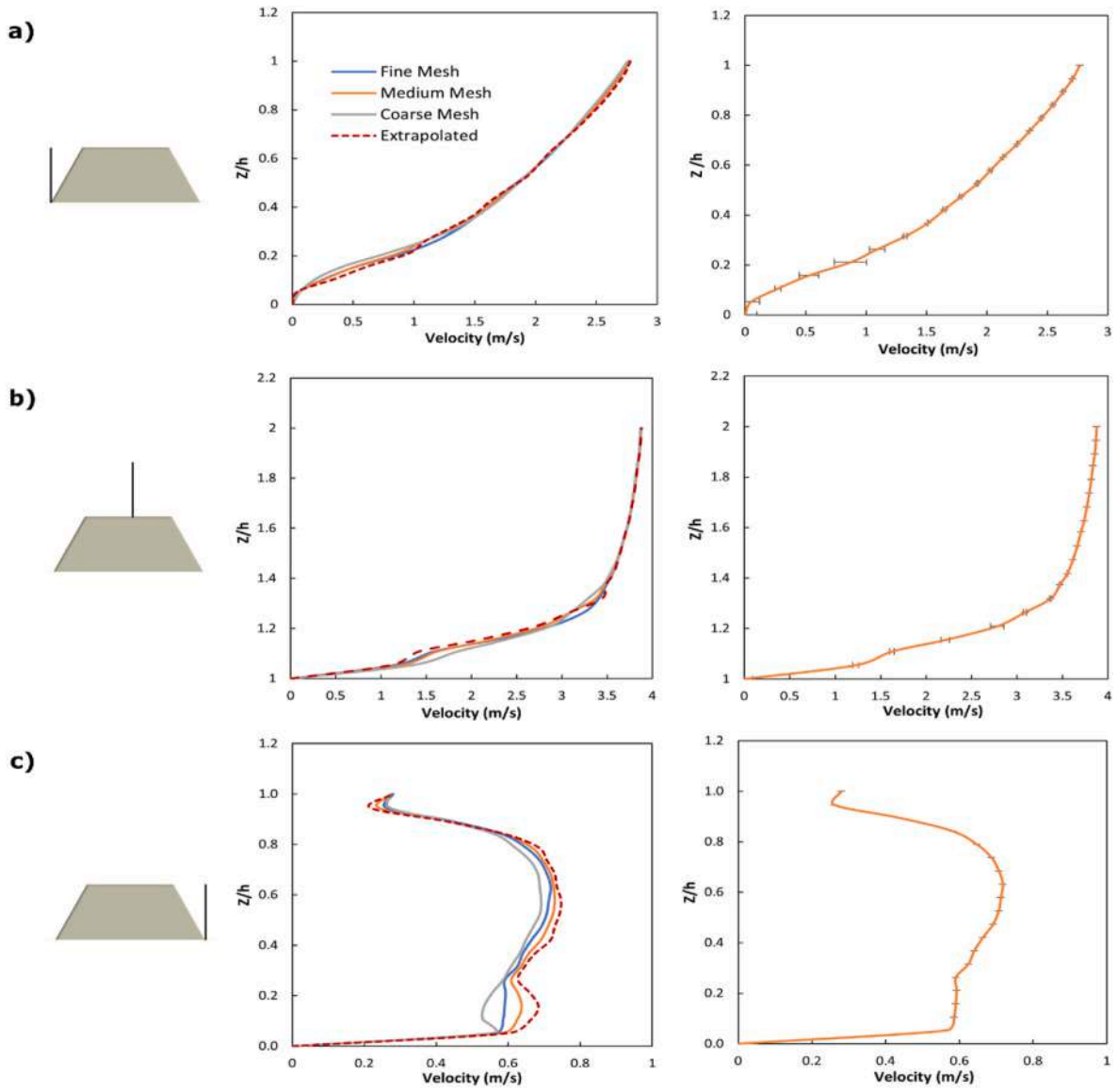

Fig. 4. Velocity profiles and error bars for grid independence study conducted (a) upstream of the pile (b) above the center of the pile, and (c) downstream of the pile.

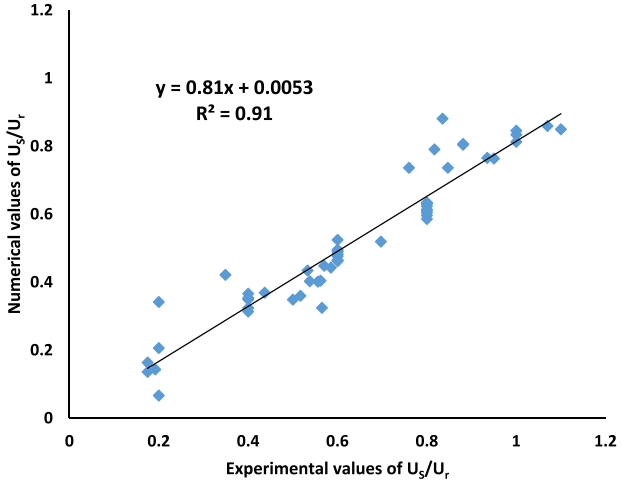

Fig. 5. Plot of modelled vs measured values of Us/Ur.

Table 1
Definitions and recommended criteria of the statistical methods compared with the calculated values for the validation model.

Metric	Definition	Recommended criteria	Statistical validation results
RNMSE	$the\ \sqrt{\overline{(C_0 + C_P)^2}/(\overline{C_0}\ \overline{C_P})}$	$< \sqrt{1.5}$	0.1389
FB	$(\overline{C_0} - \overline{C_P})/(0.5(\overline{C_O} + \overline{C_P}))$	−0.3,0.3	0.2005
FAC2	fraction of data that satisfy $0.5 \leq (C_P/C_0) \leq 2$	>0.5	0.9821
MG	$exp[\overline{ln\ C_0} - \overline{ln\ C_p}]$	0.7,1.3	1.2325
VG	$exp[\overline{(ln\ C_0 - ln\ C_p)^2}]$	<4	0.2539

C_0 observations, C_p model predictions.

then used to determine u^* (using Equation (3)). It is worth noting that the upper limit of the intervals u_s/u_r were used for the calculation.

This study has also considered the shear stress (τ) on pile surfaces to investigate the effect of the designed fence-deflectors because it is regarded as a critical force that influences dust emission from the pile

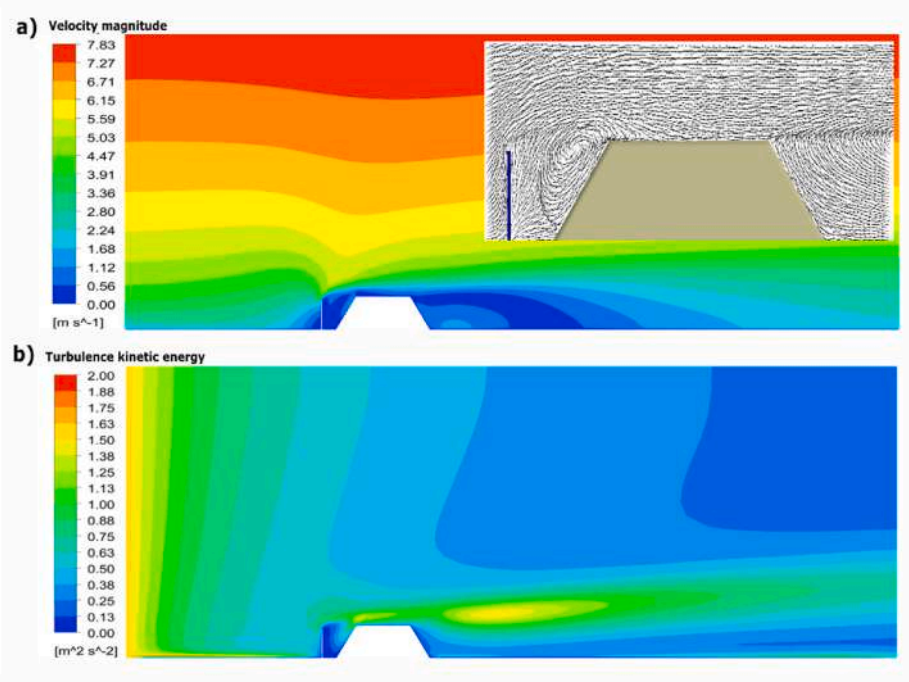

Fig. 6. (a) Velocity contour and vectors field, and (b) turbulent kinetic energy around the pile for Case 1.

surfaces (Song et al., 2014). It is defined using the following formula:

$$\tau = \rho \bullet (u^*)^2 \tag{6}$$

Where ρ is the air density, while Equation (3) has defined the friction velocity u* using the average value of u_s/u_r over the pile surface.

2.3. Numerical model description

2.3.1. Computational domain and grid

The computational domain shown in Fig. 2 comprised a cuboid of variable dimensions depending on the geometric characteristics of the pile and dynamic fence-deflector. The inlet and outlet distances between the model and the computational domain are 8 h and 20 h (where h is the pile height), respectively. The domain height is 9 h, while the lateral boundaries of the domain are 13 h in length from the pile. Those chosen domain sizes also verify the blockage ratio (BR) condition, defined by Blocken (2015) as the ratio of the model's projected frontal area to the domain's entry extent, which should be less than 3%. For the chosen dimensions, BR is 2.8%.

The computational domain was divided into 30 zones to achieve a satisfactory balance between capturing the variations in the flow field and reducing the computing time. A grid resolution was chosen for each zone. Unstructured tetrahedral cells were placed around the stockpile, solid fence and the deflector with an inflation layer applied to the walls to achieve a y + value less than/equal to 1 as is required for the wall model used by the k-ω SST turbulence model. At the same time, structured grid cells were used for the rest of the computational domain, as shown in Fig. 3.

2.3.2. Boundary conditions

The inlet condition of the computational domain was set as velocity inlet using a user-defined function. A user-defined function (UDF) was used to apply a non-uniform x-velocity on the inlet, which has a parabolic shape (as seen in Fig. 2(a)).

The mean velocity of the simulated atmospheric boundary layer (ABL) had the following power law function:

$$U = U_{ref}\left(z/z_{ref}\right)^n \tag{7}$$

U_{ref} represents the velocity at the reference height z_{ref}, and n is the power law exponent with the fitted value of $n = 0.28$ for the wind profile of an industrial site (Ray et al., 2006).

The specific dissipation rate (ω) was calculated using Equation (7), proposed by FLUENT (FLUENT, 2006) which reads,

$$\omega = k^{1/2} \Big/ \left(C_u^{1/4} \cdot l\right) \tag{8}$$

where C_μ is an empirical constant of 0.09, $l = 0.07h$ represent the length turbulence scale, and k is the turbulence kinetic energy given as follows:

$$k = \frac{3}{2}\left(U \bullet I_u\right)^2 \tag{9}$$

where I_u is the turbulence intensity.

Outlet boundaries were set as outflows, meaning the values' gradient in the direction average to the output is zero. A symmetry condition was applied to the top and lateral sides of the domain, while the stockpile, solid fence, wind deflector, and the bottom of the domain were set as walls.

2.3.3. Turbulent model and solver parameter

The paper presents CFD simulations performed in ANSYS Fluent using 3D steady-state and RANS approach with the k-ω SST turbulence model. The velocity-pressure coupling scheme was implemented using the SIMPLEC algorithm. Gradients were assessed through the Green-Gauss node-based method, and the pressure was interpolated using a second-order scheme. Second-order upwind discretisation schemes were utilised for momentum, turbulent kinetic energy, and specific dissipation rate. The residual convergence criteria were set to 10^{-6}.

2.3.4. Grid independence study

A grid independence study was performed using the grid convergence index (GCI) method. Richardson's extrapolation was used to calculate the GCI, considering coarse, medium, and fine mesh of 2156976, 3442335, and 5493648 cells, respectively.

$$GCI = \left(f_s \cdot e_a\right) / \left(r^{p-1}\right) \tag{10}$$

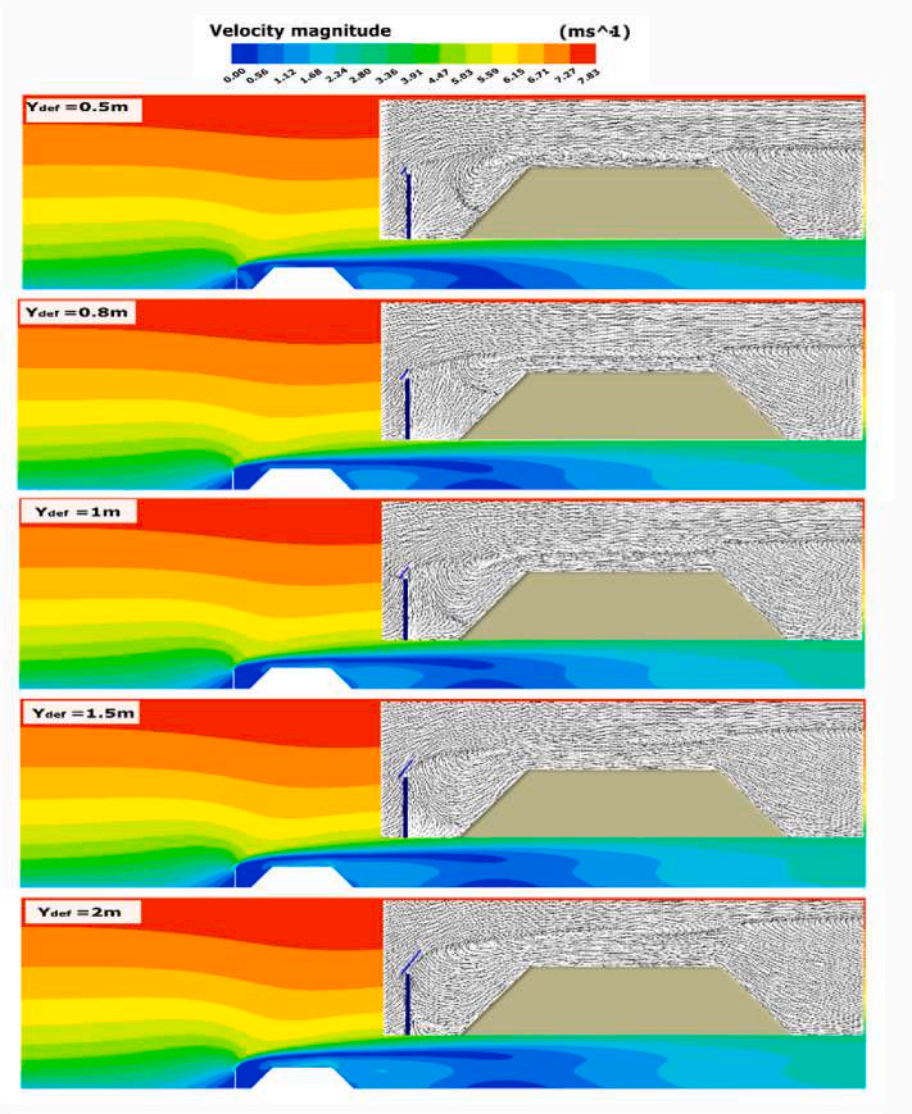

Fig. 7. Contours of velocity magnitude and velocity vectors around the pile for a 35° deflector inclination angle and different Y_{def}.

where f_s is the safety factor equal to 1.25 as recommended by Roache (1994) for three or more grids, e_a is the approximate relative error, r is the grid refinement ratio, and p is the order of convergence. The study was based on the mean wind velocity at three different positions for each grid (position (a) upstream of the pile, (b) above the center of the pile, and (c) downstream of the pile), as illustrated in Fig. 4.

Out of the three positions (a, b, and c), the average GCI that assessed the numerical solution error of the fine and medium grids were 2.9%, 1.6%, and 4.1%, respectively. This indicates that the numerical solutions produced by these grids were almost identical.

Examining the finding of those studied positions, it was observed that the velocities recorded on all three grids showed oscillatory convergence at 0.6 m/s. This behavior can be seen in Fig. 4(c). The sudden shift in behavior at this velocity and height is caused by the formation of eddies behind the leeward surface due to flow detachment and separation from the pile's crest. The recirculation zone formed at this level clarifies why all three grids follow the same trend before and after this position.

Fig. 4 demonstrates that the medium grid matched well with the extrapolated results. Hence, after evaluation, the medium grid was the most optimal and was consequently adopted for the rest of the study.

2.4. Model validation

Data from the EPA Meteorological Wind Tunnel (MWT) (Stunder and Arya, 1988; U.S. EPA, 1988) study was used to validate the numerical model. This study assessed conditions for controlling fugitive dust emissions from storage piles. The pile configuration adopted was the EPA standard oblong flatted-top pile. It was characterised by a height h of 11 m and a slope angle of 37°. The model and prototype were scaled at a ratio of 1:100. More details about the boundary conditions can be found in Badr and Harion (2005). The numerical result of normalised wind speeds U_s/U_r, where U_s is the wind speed near the pile surface (at 25 cm reel scale and 0.25 cm at WT scale) and U_r is the wind speed at the equivalent full-scale height of 10 mm. These were plotted against the EPA experimental data in Fig. 5. The ccoefficient R^2 was 0.91, which indicates a good agreement between modelled and measured values of U_s/U_r.

Various statistical performance metrics were computed to better quantify the applied CFD method's numerical accuracy, as Chang and Hanna (2004) suggested. Table 1 shows the root normalised mean square error (RNMSE = $\sqrt{\text{NMSE}}$), fractional bias (FB), fraction of predictions within a factor of 2 of the observations (FAC2), geometric mean bias (MG), and geometric mean-variance (VG). Based on Fig. 5 and the

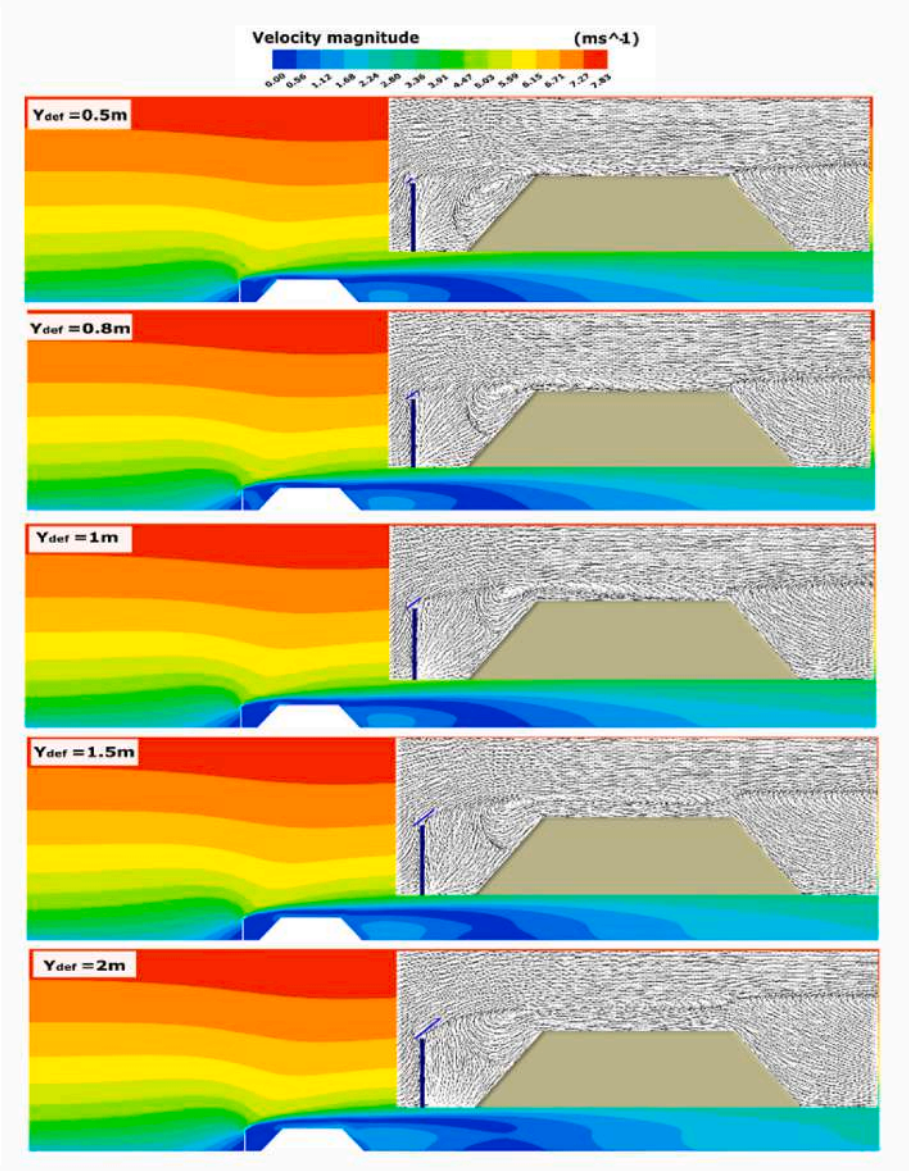

Fig. 8. Contours of velocity magnitude and velocity vectors around the pile for different Y_{def} (deflector inclination angle 50°).

statistical validation results in Table 1, the performance of the numerical model was considered highly satisfactory.

3. Results and discussion

This section discusses the results obtained in the study described above. First, the performance of the proposed dynamic fence-deflector approach is examined through Case 1, a model for a single front solid fence (reference case), and Case 2: fifteen (15) fence-deflector models composed of a solid fence and deflector of different fixed inclinations angles and heights. Then, in Case 3, models of single fences having the same height as five (5) fence-deflector models in Case 2 were studied.

3.1. Case1: Solid fence

This section analyses the effects of a solid fence of 4.5 m height, set at 3 m from the pile (0.6 h of the stockpile), on velocity magnitude, flow pattern, turbulence kinetic energy (TKE) and dust emission.

Fig. 6(a) shows the velocity contours and the velocity vector field around the pile, while Fig. 6(b) illustrates the TKE contours. The inset in Fig. 6(a) shows that two recirculation zones are created. The first one is formed between the fence and the pile, which significantly reduces the mean velocity. The second recirculation zone is formed at the leeward side of the pile due to the flow that separates from the crest. The region between the windbreak and the windward side of the pile is also characterised by a critical TKE, as shown in Fig. 6(b). Here the separated shear flow causes extremely negative velocity gradients (Lee and Kim, 1999). Thus, the air flowing down the windward slope causes material particles to either fall to the ground or be carried upwards. Those results are quite consistent with the findings of San et al. (2019), who reported the same observation for a solid fence.

3.2. Case 2: Dynamic fence-deflector

This section analyses the effect of adding a rotatable deflector on the top of a solid fence for flow patterns. Consequently, its efficiency in reducing shear stress on the pile surfaces and dust emissions was assessed.

Three fixed inclination angles for the deflector (35°, 50°, and 65°) were studied. Five deflector heights were simulated for each angle to

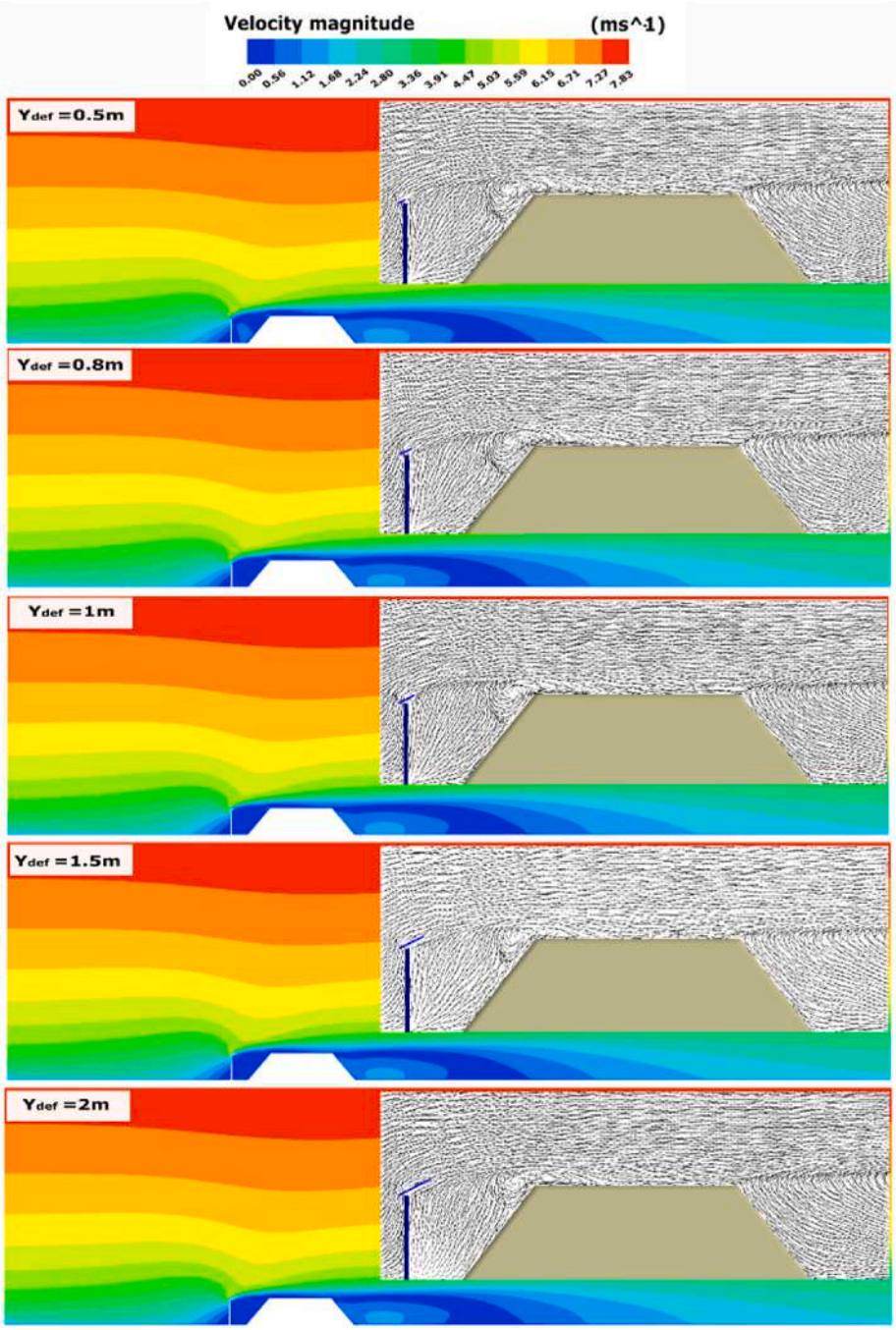

Fig. 9. Contours of velocity magnitude and velocity vectors around the pile for different Y_{def} (deflector inclination angle 65°).

determine the optimal case for reducing the emission.

3.2.1. *Deflector inclination angle 35°*

Fig. 7 presents the velocity contours and vector field for the model's pile and fence-deflector. The simulation results revealed that the wind deflector changed the original airflow pattern around the pile, where both vortex diameter and velocity magnitude behind the pile windward and top are decreased for most studied cases, as shown in Fig. 7. The velocity distribution of the designs is approximately the same in the region between the pile and the fence-deflector but much larger wind speed and recirculation flow in the wake regions as Y_{def} increases. Among the fence-deflector designs, the option with $\varnothing_{def} = 35°$ and $Y_{def} = 0.5$ m has mainly decreased the mean velocity around the pile model. In contrast, the vortex diameter and recirculating region behind the pile have shortened.

3.2.2. *Deflector inclination angle 50°*

Contour plots of mean velocity and vector velocity are depicted in Fig. 8 for the cases of $Y_{def} = 0.5$, 0.8, 1, 1.5 and 2 m (for a deflector inclination angle of 50°).

The velocity magnitude at the windward side of the pile and its top was decreased compared to the reference case for each of $Y_{def} = 0.5$, 0.8 and 1 m. For $Y_{def} = 1.5$ and 2 m the velocity magnitude has been decreased in the zone between the pile and windbreak but not on the top of the stockpile. However, all five tested Y_{def} values have reduced the vortex diameter.

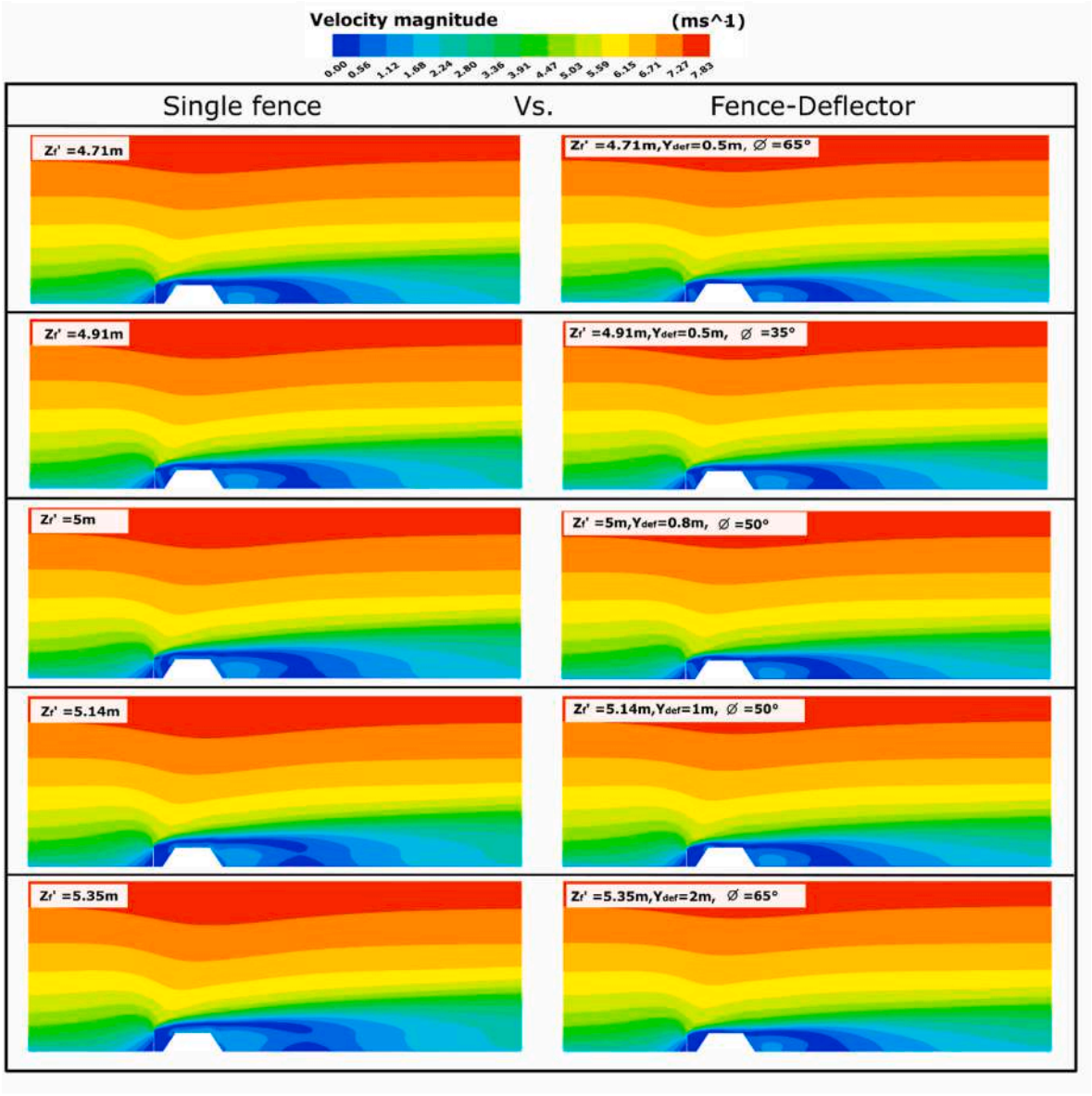

Fig. 10. Contours of velocity magnitude of single solid fences compared to velocity magnitude contours of the fence-deflector.

3.2.3. *Deflector inclination angle 65°*

Fig. 9 illustrates the variation of the velocity contours and vectors filed around the pile for the five tested Y_{def} having $\varnothing_{def} = 65^{\circ}$.

The velocity magnitude on both the top pile and behind the piles windward side was decreased for the five different Y_{def}, as shown in Fig. 9. However, velocity contours on the leeward surface are stable despite changes in Y_{def}, likely due to a low-speed recirculation downstream of the stockpile. Interestingly, as Y_{def} increases, the vortex diameter between the fence-deflector and the windward surface of the pile can be reduced, compared to the reference case Fig. 6(a). Among the tested models with different Y_{def}, the design with $\varnothing_{def} = 65^{\circ}$ and $Y_{def} = 2$ m resulted in the optimal reduction of mean velocity around the pile model, as well as a decrease in vortex diameter and a shorter recirculating region on the leeward side of the pile.

3.3. *Case3: single solid fences*

Figs. 10 and 11 compare the velocity contour distributions and the velocity vectors around the pile for the cases of single solid fences against the cases of the fence-deflector having the same height ($Z_f' = Z_f + Z_{def}$). The objective was to compare simply increasing the height of a single solid fence to adding a dynamic deflector on an existing solid fence. Fig. 10 shows two recirculation regions, also found by (Chen et al., 2012). The first was formed between the fence and pile's windward surface, while the second recirculation zone was formed behind the leeward surface, characterised by a more significant extent than the first one. This recirculation is probably caused by the flow separating from the pile's crest.

In addition, in Fig. 10, it was observed that the velocity magnitude on both the zone between the pile and fence-deflector and on the top of the stockpile was reduced by the fence-deflector. Moreover, using fence-deflectors reduced the recirculation flow scale in the wake region, causing less impact on the leeward surface of the piles compared to using single fences. Besides, the flow recirculation between the pile and the solid fence was reduced when the deflector was installed on the top. As a result, the intensity and diameter of the vortex were smaller than in cases with a single solid fence, according to Fig. 11. Thus, the piles windward slope is more protected and less subject to material particle blows and dust emission.

Contours of the TKE distributions for single solid fences and the

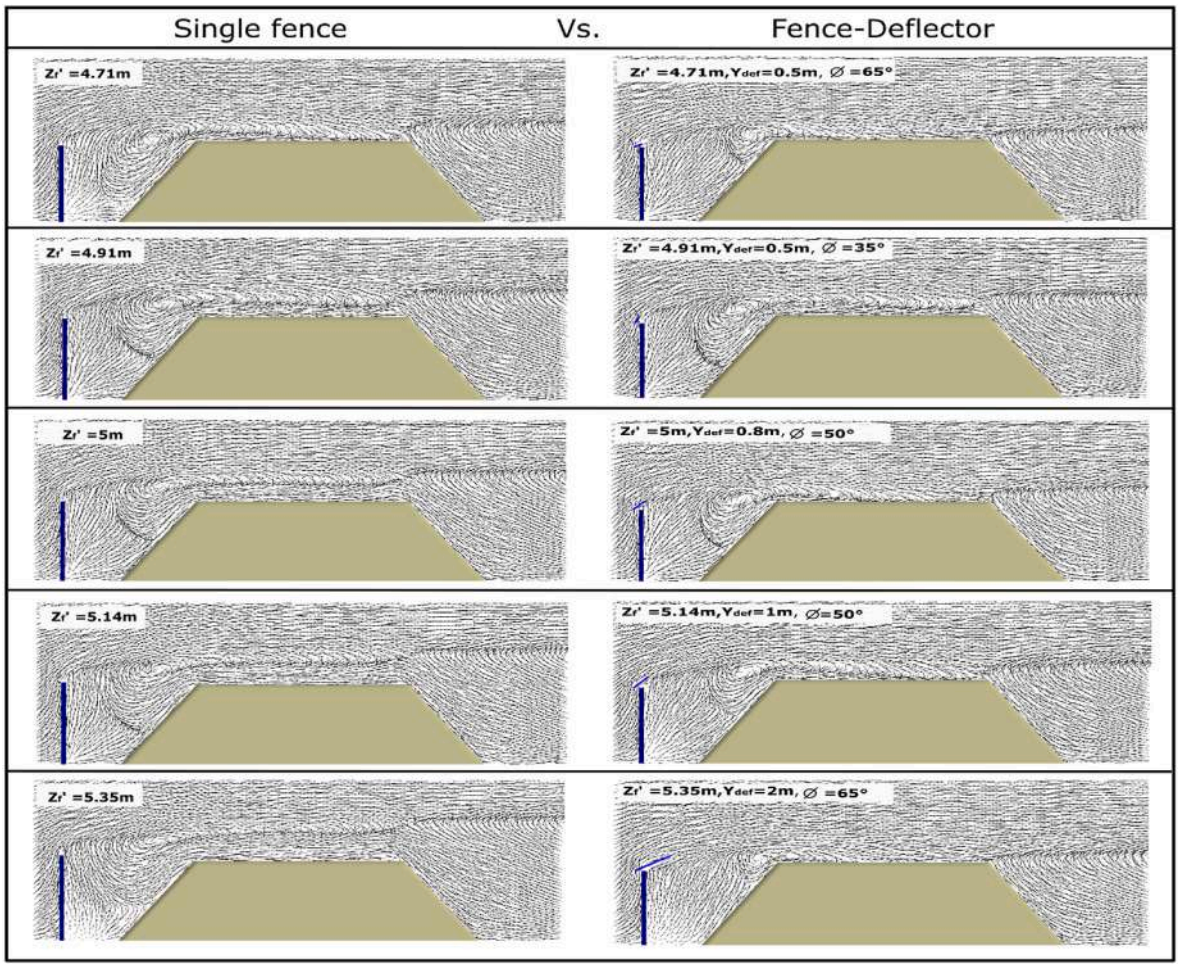

Fig. 11. Velocity vector fields around the pile behind single solid fences compared to velocity vector fields behind the fence-deflector.

fence-deflector are shown in Fig. 12.

It is observed that a large TKE above the pile was generated in the cases of the single fence, and this evolved subsequently in the leeward region behind the stockpile. TKE increases as the height of the single solid fence increases. As an illustration, when the height of the fence is increased from 4.51 m to 5.35 m, the TKI increases from 1.38 m^2s^{-2} to 2 m^2s^{-2}, on the top surface of the pile. This is because the shear flow separated from the fence hits the top of the windward pile surface, causing an increase in TKE in this region (San et al., 2019). Adding the deflector lifted this from the pile surface, reducing the separated flow from the fence top and the TKE. The TKE also vastly reduces the size of the recirculation zone between the pile and fence-deflector compared to the single fences. Moreover, it is essential to note that for the deflector characterised by $\varnothing_{def} = 65^\circ$ and $Y_{def} = 2$ m, the TKE is almost equal to zero in the zone between the pile and fence-deflector compared to the other models. Also, the TKE on the top of the stockpile was reduced by 50% (2 m^2s^{-2} for the single fence against 1 m^2s^{-2} for the fence-deflector). This drop in TKE is because this specific fence-deflector design was characterised by the small vortex diameter in the windward pile, as shown in Fig. 11.

To better demonstrate the role of the deflector in reducing the recirculation zones, as shown before in Figs. 10 and 11, the simulated velocity streamlines are presented in Fig. 13 for the solid fence of $Z_f' = 5.35$ m and the fence-deflector with $\varnothing_{def} = 65^\circ$ and $Y_{def} = 2$ m (having the same equivalent height $Z_f' = 5.35$).

The fence-deflector has been observed to reduce the flow recirculation between the pile and the solid fence, resulting in a smaller intensity and diameter of the vortex than in cases with a single solid fence, as shown in Fig. 13. Additionally, the size of the flow recirculation on top of the stockpile and in the pile leeward side was also reduced, resulting in less impact on the top and downwind surface of the piles compared to using a single solid fence. Furthermore, the fence-deflector reduced the velocity magnitude in both the zone between the pile and the fence-deflector and on top of the stockpile. This result supports the findings presented in Figs. 10 and 11, indicating that the dynamic deflector added on the top of a solid fence is much more effective than using only a solid fence.

3.4. Shear stress and dust emission

This section presents the quantitative analysis of the shear stress on the piles surface and and the consequent effect on dust emission.

The dust emission was calculated using the USEPA model presented in section 2.2. An example of the contours of the velocity ratio u_s/u_r over the stockpiles obtained by the 3D numerical simulations for the solid fence of $Z_f' = 5.35$ m and the fence-deflector $\varnothing_{def} = 65^\circ$ and $Y_{def} = 2$ m (having the same equivalent height) is shown in Fig. 14. The same process has been carried out for all the studied cases to estimate the contribution to the emission of each sub-area for each pile configuration (to be used in Equations (3)–(5)).

Table 2 reports the mean shear stress and dust emission factors (EF) for Case 1 and each studied model of Case 2.

To better emphasise the role of the dynamic deflector, the estimated mean shear stress on the surface pile and EF of the tested single solid fences compared to the designed fence-deflectors having the same equivalent height (Case 3) are reported in Fig. 15.

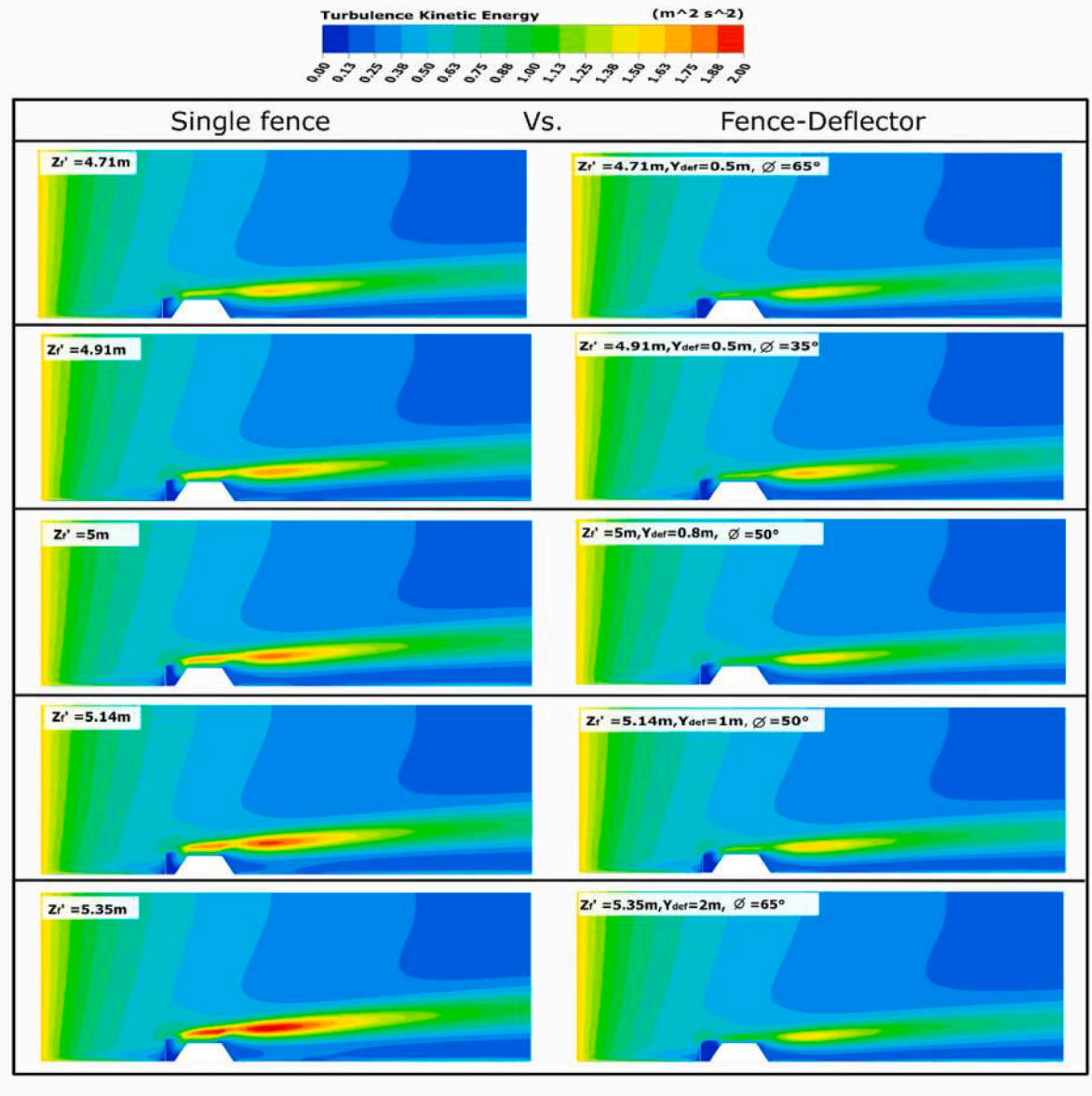

Fig. 12. Contours of Turbulence kinetic energy for single solid fences compared to turbulence kinetic energy contours for the fence-deflector.

3.4.1. *Shear stress*

According to the data in Table 2, the fence-deflector models with $\varnothing_{def} = 35^{\circ}$ registered lower shear stress values for the cases with $Y_{def} =$ 0.5 and 0.8 m than the solid fence alone. At the same time, the models having $\varnothing_{def} = 50^{\circ}$ recorded lower shear stress values for each of $Y_{def} =$ 0.5, 0.8, 1 and 1.5 m cases. On the other hand, in the fence-deflector models with $\varnothing_{def} = 65^{\circ}$, the shear stress has been lowered for all tested Y_{def}. The design with $Y_{def} = 1$ m and $\varnothing_{def} = 50^{\circ}$ was the most efficient and registered the smallest shear stress value among the tested models. This model decreased the shear stress on the pile surface by 38.23% (from 39.15 Pa for the reference case to 24.18 Pa).

For the cases with $\varnothing_{def} = 35^{\circ}$, the shear stress increases with the increase of Y_{def}. These results could be justified by the fact that the displaced flow speed and the extent of the second recirculation zone slowly increase as the height of the fence-deflector Z_f' increases, as shown in Figs. 10 and 11. In contrast, for the cases with $\varnothing_{def} = 60^{\circ}$, the model having the highest Y_{def} (2 m) registered the lowest shear stress value (compared to the other models of the same $\varnothing_{def}$) which means that it is not affected by the increase of Z_f'. The reason is that the second recirculation zone decreases as Y_{def} increases. For example, for the case $\varnothing_{def} = 65^{\circ}$ and $Y_{def} = 2$ m, the first recirculation zone almost disappears while the width of the second recirculation is considerably reduced. The high $\varnothing_{def}$ angle and Y_{def} inhibited the formation of the recirculation zone, hence the reduced shear stress (the particle uptake) and the emission factor.

The estimated shear stress on the surface of the pile for single solid fences compared to the designed fence-deflectors having the same equivalent height (see Fig. 15), demonstrates that the fence-deflector models reduced the shear stress compared to the cases of single fences. Those results emphasise the positive performance of the new fence-deflector design in reducing dust emissions by lessening the shear stress.

3.4.2. *Emission factor (EF)*

As shown in Tables 2 and in the fence-deflector models with $\varnothing_{def} =$ 35°, the EF decreased for $Y_{def} = 0.5$ and 0.8 m compared to the reference case and increased as the deflector height increased for the rest of the tested Y_{def} (1, 1.5 and 2 m). On the other hand, the fence-deflector models with $\varnothing_{def} = 50^{\circ}$ registered a reduction of EF for the cases Y_{def} $= 0.5$, 0.8, 1 and 1.5 m compared to the reference case. At the same time, EF increased for $Y_{def} = 2$ m, as observed in Table 2. The design with Y_{def}

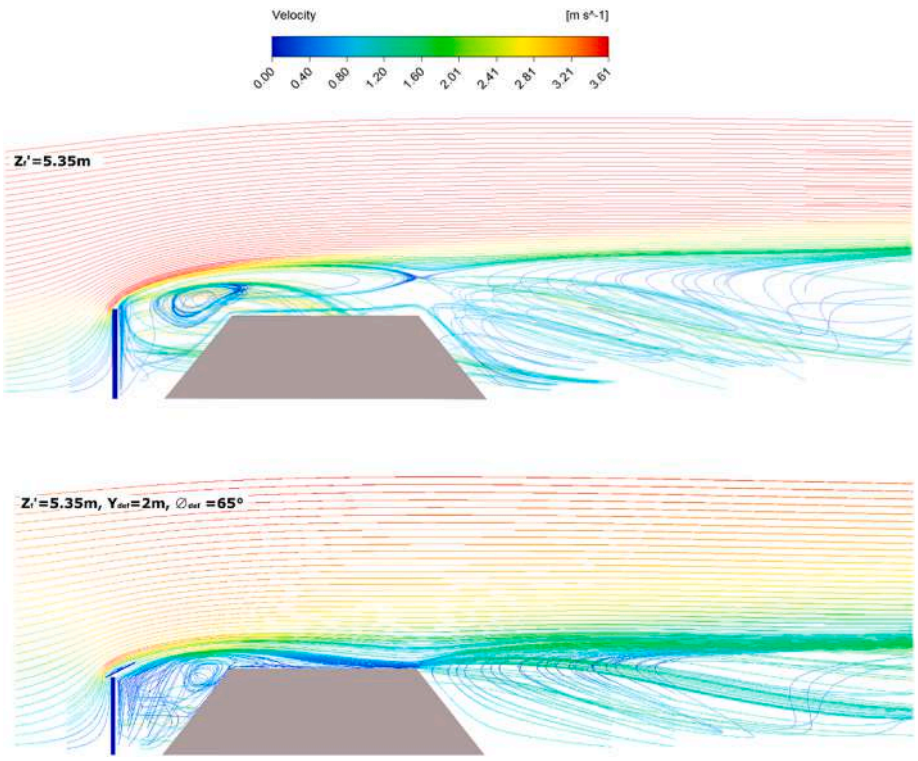

Fig. 13. Velocity streamlines for the solid fence of Z_f' = *5.35 m and the fence-deflector* $\varnothing_{def} = 65^\circ$ *and* $Y_{def} = 2$ *m.*

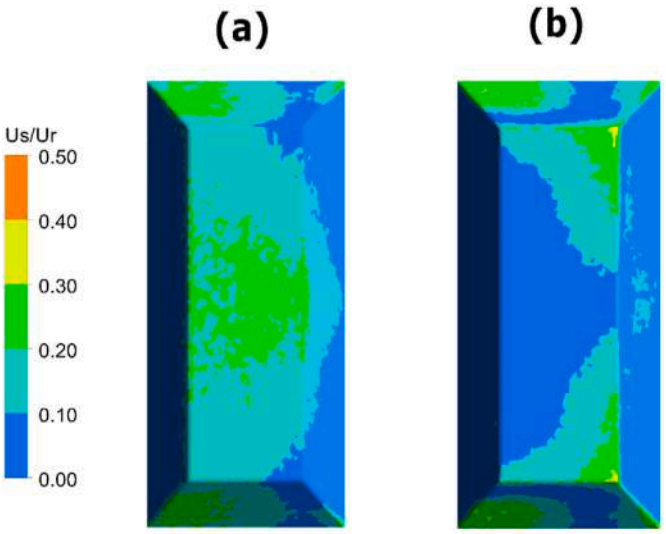

Fig. 14. Contours of the velocity ratio u_s/u_r over the stockpiles a) single solid fence (Z_f' = 5.35 m) and b) fence deflector with $\varnothing_{def} = 65^\circ$ and $Y_{def} = 2$ m (Z_f' = 5.35 m).

= 1 m was the most efficient and registered the smallest EF among the tested Y_{def} under $\varnothing_{def} = 50^\circ$. The EF was reduced by 18.02% compared to the reference case (Case 1). These outcomes explain the result illustrated in Fig. 8, where the design with $Y_{def} = 1$ m primarily decreased the velocity around the pile model and reduced the vortex diameter compared to the other tested design of the same angle ($\varnothing_{def} = 50^\circ$).

Conversely, the five deflectors having $\varnothing_{def} = 65^\circ$ and Y_{def} varying from 0.5 to 2 m reduced the emission factor. The most effective design was Y_{def} = 2 m, which recorded an emission factor of 1098.36 g/disturbance against 1309.86 g/disturbance for the reference case (a reduction on EF of 16.14%). For Case 3, the designed fence-deflectors reduced the emission factor compared to the cases of single fences for all the tested $\varnothing_{def}$ and Y_{def}, as outlined in Fig. 15.

Overall, the reported results in Table 2 and Fig. 15 emphasise the role of $\varnothing_{def}$ and Y_{def} and the positive performance of the new fence-deflector design in reducing shear stress, and thus dust emissions from an open storage pile.

To summarize, the above results for the different studied cases affirm that the new fence-deflector, compared to the single fence models, can minimise the velocity magnitude on both the zone between the pile and fence-deflector, and the top of the stockpile. Similarly, the turbulence intensity was vastly reduced. Thus, the vortex intensity and diameter were lessened. Furthermore, the recirculating flow between the fence and the pile was reduced when the deflector was installed on the top of the fence. In addition, the large-scale recirculation flow in the leeward pile sides has also been reduced, which means that both the windward and the leeward sides of the pile are less affected in fence-deflector cases than for single solid fences.

The dynamic fence-deflector design has proven to be highly efficient in reducing dust emissions from open storage piles compared to single solid fences. This design offers a promising solution for controlling dust emissions in industrial environments. Yet, realising these benefits hinges on navigating real-world challenges with precision. Further research is required to develop practical guidance on the implementation of a system of this kind. The present study represents an early proof of concept, yet in practice the specifications of the wind deflector (height, position, adaptability, etc.) would require case-specific design. Adaptability can be ensured by the dynamic adjustments of the automated systems capable of real-time adjustments based on wind speed/direction and stockpile configurations to enhance overall efficiency. This would require the installation of local sensors, data communication and collection systems, and a control algorithm which can optimise the decision of deflector orientation. However, each of these aspects requires further research and technological development.

In addition, industries should prioritise critical considerations to ensure practicality, longevity, and operational feasibility. Regarding material selection and durability, opting for corrosion-resistant

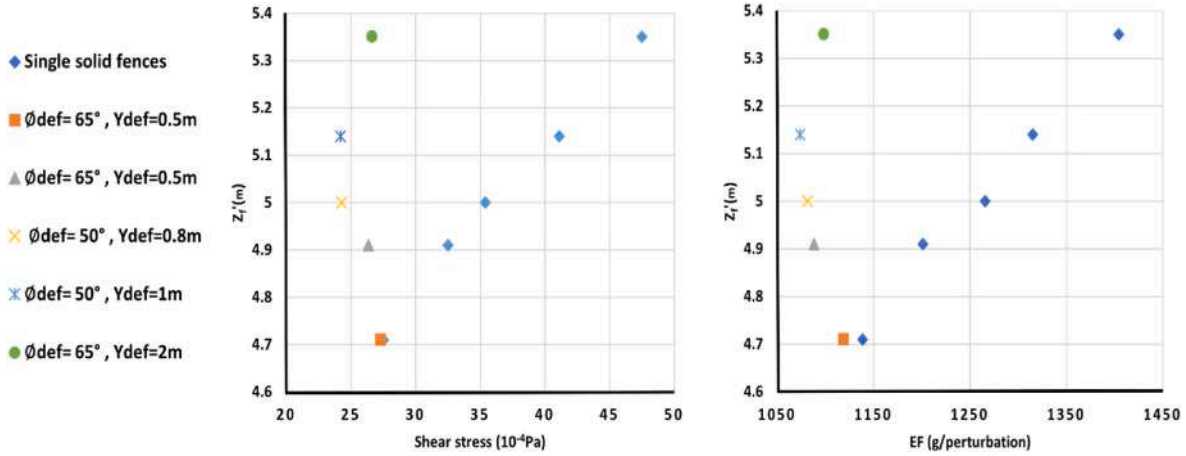

Fig. 15. Mean shear stress on the surface pile and Emission factors for each single solid fence and the fence-deflector of the same height (Z_f').

Table 2
Mean shear stress and emission factors for the Case 1 and Case 2.

	$\varnothing_{def\ i}$	$Y_{def\ i}$ (m)	Z_f' (m)	Mean shear stress 10^{-4} (Pa)	EF (g/ perturbation)
Case1: ***Solid Fence only*** $Z_f = 4.5$ ***m***	/	/	**4.5**	39.15	1309.86
Case 2: ***Solid fence*** $Z_f = 4.5$ ***m*** + ***Deflector*** $\varnothing_{def\ i}$ ***and*** $Y_{def\ i}$	**35°**	**0.5**	**4.91**	26.35	1088.24
		0.8	**5.16**	35.41	1271.04
		1	**5.32**	41.78	1322.17
		1.5	**5.73**	49.86	1444.28
		2	**6.14**	59.09	1605.35
	50°	**0.5**	**4.82**	34.79	1245.93
		0.8	**5.01**	24.28	1081.17
		1	**5.14**	24.18	1073.78
		1.5	**5.46**	32.86	1215.76
		2	**5.79**	45.53	1386.24
	65°	**0.5**	**4.71**	27.32	1119.01
		0.8	**4.84**	28.87	1139.72
		1	**4.92**	29.31	1147.07
		1.5	**5.13**	33.58	1226.55
		2	**5.35**	26.64	1098.36

materials capable of withstanding harsh environmental conditions is paramount. Regular structural assessments, incorporated into a robust maintenance schedule, are essential to detect and promptly address signs of wear and tear. Lastly, monitoring systems and data analysis, which enable continuous performance tracking, can also inform proactive maintenance strategies. By meticulously addressing these facets, industries can optimise the effectiveness and sustainability of dynamic wind deflector systems, overcoming challenges tied to maintenance, durability, and operational feasibility.

4. Conclusion

The present study introduces a new windbreak design composed of a solid fence and rotatable wind deflector. The effect of the fence-deflector on the airflow structure and its performance in reducing the emission of dust from open storage piles have been studied numerically, by employing 3D CFD simulations and then implementing the USEPA emission model for industrial wind erosion. The numerical simulation used the RANS *k-ω* SST turbulence model. The simulation model was validated against wind tunnel experimental data from the EPA to ensure accuracy.

The results have shown that adding a movable deflector on the top of a solid fence significantly reduces the flow velocity and TKE on the windward side of the pile. As a result, it minimises the recirculation flow on the leeward side (the wake region). In addition, the vortex growth and diameter on the area between the pile and the fence-deflector have been reduced. Additionally, the findings indicate that overall, the windbreak with a fence-deflector of $Y_{def} = 2$ m and $\varnothing_{def} = 65°$ performs better than the other tested fence-deflector configurations in reducing the shear stress and emissions on the pile surfaces and thus the emission of dust. The comparisons between this optimum case and the single solid fence (having the same height) highlighted a reduction of 29.16% in the shear stress and 21.79% in the emission. This result also illustrates that it is possible to optimise the deflector angle for changing ambient or operational conditions (i.e., a dynamic system which responds to changes in wind speed, direction, or pile height).

The study outcomes indicate that the dynamic deflector added on the top of a solid fence is significantly more efficient than a single solid fence. Although the design variables considered in this study are limited to one pile shape and wind flow velocity, the present work may serve as a starting point for further work to develop a fully automated dynamic fence-deflector system capable of optimising dust emissions control in all physical scenarios and ambient conditions. Future research is required to investigate particle dust emission modelling and fence-deflector performance to reduce dust emission from various storage pile shapes, accounting for multiple piles, complex pile shapes, typical industrial configurations, and dynamic weather conditions.

Funding

This research received no external funding.

CRediT authorship contribution statement

Ouiza Bouarour: Conceptualization, Data curation, Formal analysis, Methodology, Software, Validation, Visualization, Writing – original draft, Writing – review & editing. **Aonghus McNabola:** Conceptualization, Methodology, Resources, Supervision, Validation, Visualization, Writing – review & editing. **Battista Grosso:** Methodology, Supervision, Visualization, Writing – review & editing. **Brian Considine:** Visualization, Writing – review & editing. **Alessio Lai:** Writing – review & editing. **Francesco Pinna:** Writing – review & editing. **Valentina Dentoni:** Methodology, Resources, Supervision, Validation, Visualization, Writing – review & editing.

Declaration of competing interest

The authors declare that they have no known competing financial

interests or personal relationships that could have appeared to influence the work reported in this paper.

Data availability

Data will be made available on request.

Acknowledgements

Research carried out in the framework of projects conducted by CESA (Centre of Excellence on environmental sustainability, Sardinia, Italy) and CINIGeo (National Interuniversity Consortium for Geo-resources Engineering between the University of Bologna, Cagliari, Rome "La Sapienza" and Trieste, Italy).

References

Alghamdi, A.A., Al-Kahtani, N.S., 2005. Sand control measures and sand drift fences. J. Perform. Constr. Facil. 19 (4), 295–299. https://doi.org/10.1061/(ASCE)0887-3828, 2005)19:4(295.

Badas, M.G., Dentoni, V., Angius, F., Pinna, F., 2022. Numerical investigation on the PM emission potential of metal sulphides open storage. Atmosphere 13 (9), 1417. https://doi.org/10.3390/atmos13091417.

Badr, T., Harion, J.L., 2005. Numerical modelling of flow over stockpiles: implications on dust emissions. Atmos. Environ. 39 (30), 5576–5584.

Badr, T., Harion, J.-L., 2007. Effect of aggregate storage piles configuration on dust emissions. Atmos. Environ. 41 (2) https://doi.org/10.1016/j.atmosenv.2006.07.038. Article 2.

Blocken, B., 2015. Computational Fluid Dynamics for urban physics: importance, scales, possibilities, limitations and ten tips and tricks towards accurate and reliable simulations. Build. Environ. 91, 219–245. https://doi.org/10.1016/j.buildenv.2015.02.015.

Bruno, L., Horvat, M., Raffaele, L., 2018. Windblown sand along railway infrastructures: a review of challenges and mitigation measures. J. Wind Eng. Ind. Aerod. 177, 340–365. https://doi.org/10.1016/j.jweia.2018.04.021.

Chang, J.C., Hanna, S.R., 2004. Air quality model performance evaluation. Meteorology and Atmospheric Physics 87 (1–3). https://doi.org/10.1007/s00703-003-0070-7.

Chen, G., Wang, W., Sun, C., Li, J., 2012. 3D numerical simulation of wind flow behind a new porous fence. Powder Technol. 230, 118–126.

Cong, X.C., Yang, S.L., Cao, S.Q., Chen, Z.L., Dai, M.X., Peng, S.T., 2012. Effect of aggregate stockpile configuration and layout on dust emissions in an open yard. Appl. Math. Model. 36 (11), 5482–5491.

Dentoni, V., Grosso, B., Pinna, F., Lai, A., Bouarour, O., 2022. Emission of fine dust from open storage of industrial materials exposed to wind erosion. Atmosphere 13 (2), 320.. https://doi.org/10.3390/atmos13020320.

Diego, I., Pelegry, A., Torno, S., Toraño, J., Menendez, M., 2009. Simultaneous CFD evaluation of wind flow and dust emission in open storage piles. Appl. Math. Model. 33 (7), 3197–3207. https://doi.org/10.1016/j.apm.2008.10.037.

Dong, Z., Luo, W., Qian, G., Wang, H., 2007. A wind tunnel simulation of the mean velocity fields behind upright porous fences. Agric. For. Meteorol. 146 (1), 82–93. https://doi.org/10.1016/j.agrformet.2007.05.009.

Dong, Z., Qian, G., Luo, W., Wang, H., 2006. Threshold velocity for wind erosion: the effects of porous fences. Environ. Geol. 51 (3), 471–475. https://doi.org/10.1007/s00254-006-0343-9.

Ferreira, A.D., Lambert, R.J., 2011. Numerical and wind tunnel modeling on the windbreak effectiveness to control the aeolian erosion of conical stockpiles. Environ. Fluid Mech. 11 (1), 61–76. https://doi.org/10.1007/s10652-010-9176-x.

Ferreira, M.C.S., Furieri, B., Santos, J.M., El Moctar, A.O., Harion, J.-L., Valance, A., Dupont, P., Reis, N.C., 2020. An experimental and numerical study of the aeolian erosion of isolated and successive piles. Environ. Fluid Mech. 20 (1), 123–144. https://doi.org/10.1007/s10652-019-09702-z.

FLUENT, 2006. FLUENT User's Guide V6, vol. 2.

Furieri, B., Russeil, S., Harion, J.L., Santos, J., Milliez, M., 2012. Comparative analysis of dust emissions: isolated stockpile vs two nearby stockpiles. Air Pollution 285–294.

Hassan, H., Abraham, M., Kumar, P., Kakosimos, K.E., 2017. Sources and emissions of fugitive particulate matter. In: AIRBORNE PARTICLES, p. 21.

Lee, S.-J., Kim, H.-B., 1999. Laboratory measurements of velocity and turbulence field behind porous fences. J. Wind Eng. Ind. Aerod. 80 (3), 311–326.

Lee, S.-J., Lim, H.-C., 2001. A numerical study on flow around a triangular prism located behind a porous fence. Fluid Dynam. Res. 28 (3), 209. https://doi.org/10.1016/S0169-5983(00)00030-7.

Lv, P., Dong, Z., Luo, W., Qian, G., 2013. The pressure-field characteristics around porous wind fences: results of a wind tunnel study. Environ. Earth Sci. 68 (4), 947–953. https://doi.org/10.1007/s12665-012-1797-6.

Ning, Z., Ting-guo, C., Lee, Sang-joon, 2011. Wind tunnel observation on the effect of a porous fence on shelter of a triangular coal pile. Journal of Experiments in Fluid Mechanics 25 (4), 50–54. https://doi.org/10.3969/j.issn.1672-9897.2011.04.010.

Novak, L., Bizjan, B., Pražnikar, J., Horvat, B., Orbanic, A., Širok, B., 2015. Numerical modeling of dust lifting from a complex-geometry industrial stockpile. Strojniški Vestnik - Journal of Mechanical Engineering 61. https://doi.org/10.5545/sv-jme.2015.2824.

Qiu, Y., San, B., He, H., Zhao, Y., 2021. Surrogate-based aerodynamic optimization for enhancing the shelter effect of porous fences on a triangular prism. Atmos. Environ. 244, 117922 https://doi.org/10.1016/j.atmosenv.2020.117922.

Qiu, Y., Yuan, Y., Yu, R., Liu, J., 2022. Aerodynamic shape optimization of porous fences with curved deflectors using surrogate modelling. Optim. Eng. https://doi.org/10.1007/s11081-022-09777-6.

Ray, M.L., Rogers, A.L., McGowan, J.G., 2006. Analysis of Wind Shear Models and Trends in Different Terrains. University of Massachusetts, Department of Mechanical and Industrial Engineering, Renewable Energy Research Laboratory.

Roache, P.J., 1994. Perspective: A Method for Uniform Reporting of Grid Refinement Studies. Journal of Fluids Engineering 116 (3), 405–413. https://doi.org/10.1115/1.2910291.

San, B., Zhao, Y., Qiu, Y., 2019. Numerical simulation and optimization study of surface pressure and flow field around a triangular prism behind a porous fence. Environ. Fluid Mech. 19 (4), 969–987. https://doi.org/10.1007/s10652-019-09695-9.

Song, C.-F., Peng, L., Cao, J.-J., Mu, L., Bai, H.-L., Liu, X.-F., 2014. Numerical simulation of airflow structure and dust emissions behind porous fences used to shelter open storage piles. Aerosol Air Qual. Res. 14 (6), 1584–1592. https://doi.org/10.4209/aaqr.2013.11.0331.

Stunder, B.J.B., Arya, S.P.S., 1988. Windbreak effectiveness for storage pile fugitive dust control: a wind tunnel study. JAPCA 38 (2), 135–143. https://doi.org/10.1080/08940630.1988.10466360.

Torano, J.A., Rodriguez, R., Diego, I., Rivas, J.M., Pelegry, A., 2007. Influence of the pile shape on wind erosion CFD emission simulation. Appl. Math. Model. 31 (11), 2487–2502. https://doi.org/10.1016/j.apm.2006.10.012.

Torshizi, M.R., Miri, A., Shahriari, A., Dong, Z., Davidson-Arnott, R., 2020. The effectiveness of a multi-row Tamarix windbreak in reducing aeolian erosion and sediment flux, Niatak area, Iran. J. Environ. Manag. 265, 110486 https://doi.org/10.1016/j.jenvman.2020.110486.

Turpin, C., Harion, J.-L., 2010. Effect of the topography of an industrial site on dust emissions from open storage yards. Environ. Fluid Mech. 10 (6), 677–690.

U.S. EPA, 1988. Update of Fugitive Dust Emissions Factors in AP-42. Midwest Research Institute. Kansas City, *AP-42 section 11.2*—Wind erosion, MRI No. 8985-K.

U.S. EPA, 2006. Update of Fugitive Dust Emissions Factors in AP-42 Section 13.2.5 – Wind Erosion. Midwest Research Institute, Kansas City.

WRAP, 2006. WRAP Fugitive Dust Handbook, vol. 91361. Western Governors' Association, Denver, CO, USA, p. 242.

Yeh, C.-P., Tsai, C.-H., Yang, R.-J., 2010. An investigation into the sheltering performance of porous windbreaks under various wind directions. J. Wind Eng. Ind. Aerod. 98 (10), 520–532. https://doi.org/10.1016/j.jweia.2010.04.002.

Yen, P.-H., Chen, W.-H., Yuan, C.-S., Tseng, Y.-L., Lee, J.-S., Wu, C.-C., 2021. Exploratory investigation on the suppression efficiency of fugitive dust emitted from coal stockpile: comparison of innovative atomizing and traditional spraying technologies. Process Saf. Environ. Protect. 154, 348–359. https://doi.org/10.1016/j.psep.2021.08.026.

Yonkofski, C.M., Appriou, D., Downs, J.L., 2019. Dust Control Planning. Pacific Northwest National Lab.(PNNL), Richland, WA (United States).